AIAA 99-0763

DATA-BASED AERODYNAMIC MODELING USING NONLINEAR INDICIAL THEORY

Patrick H. Reisenthel‡ and Matthew T. Bettencourt¶
Nielsen Engineering & Research, Inc.
Mountain View, CA

ABSTRACT

Nonlinear indicial response theory addresses the need for high-fidelity prediction of nonlinear phenomena such as unsteady aerodynamics. The present paper describes a particular implementation of nonlinear indicial theory in which it is assumed that the indicial and critical-state responses of a nonlinear system can be parameterized based on the instantaneous motion state. These parameterized indicial and critical-state responses form a kernel which can be determined in principle from experiment, computation, or analysis. The application described in this paper considers a 65-degree delta wing undergoing forced roll oscillations at a high angle of attack. A new extraction algorithm is applied to identify the system's kernel of indicial and critical-state responses. It is shown that, using this kernel, one can accurately predict the unsteady aerodynamic response of the wing to novel maneuvers.

NOMENCLATURE

Symbols and abbreviations

b	Wing span (1.90 ft)
c	Wing chord
C_l	Rolling moment coefficient
CS	Critical State
CSR	Critical State Response
f	Frequency
IPS	Indicial Prediction System
IR	Indicial Response
M	Mach number
NIR	Nonlinear Indicial Response
sgn	Sign
t	Time
U_∞	Freestream velocity (330 ft/s)
$\delta C_l/\delta\phi$	Indicial response of rolling moment with respect to roll angle
Δf	Build-up of generic aerodynamic load, f
Δf^{CS}	Critical-state response of f
ϕ	Roll angle
σ	Body axis with respect to the freestream
τ	Auxiliary time variable
$f_j(t)$	Basis function

Subscript and Superscripts

c	Critical
CS	Critical State
DR	Deficiency Response
dyn	Dynamic
QS	Quasi-static
∞	Time-asymptotic value (except for U_∞)
•	Derivative with respect to time

1. BACKGROUND

Flight simulation is playing an increasingly important role in the development of new aircraft systems. To uncover potential problems during the early design phase requires efficient high-fidelity modeling of nonlinear aerodynamic phenomena such as unsteady flow separation, shock movement, and vortex bursting at high angles of attack. Future uninhabited combat air vehicles (UCAV) will take advantage of high dynamic lift and can be expected to experience high g's, thus increasing the importance of capturing nonlinear unsteady aerodynamic phenomena. Present aerodynamic models used in stability and control analysis are based to a large extent on linear representations which are, at best, quasi-steady and which cannot adequately model the nonlinearities associated with post-stall aerodynamics, including bifurcations and hysteresis. Thus, there is a need to enhance current flight simulation capabilities using rapid nonlinear aerodynamic math models capable of representing these effects. Recent studies suggest (Refs. 1-6) that this need can be fulfilled by using nonlinear indicial response (NIR) models.

‡ Chief Scientist, Member AIAA
¶ Research Scientist. Presently at University of Southern Mississipi.

The work of Reference 1 showed the feasibility of using nonlinear indicial theory as a viable tool for rapid unsteady aerodynamic prediction. A model was developed to predict the unsteady aerodynamic loads associated with flight maneuvers at high angles of attack and high pitch rates. This model was based on key simplifications of nonlinear indicial theory and on efficient parameterizations of the indicial and critical-state responses. To reduce the *a priori* unknown effects due to prior motion history, parameterizations based only on "local" information, such as the instantaneous angle of attack and pitch rate, were introduced. The resulting method was validated (Refs. 2,3) against two nonlinear systems. The first system (Ref. 7) modeled "Cobra"-type flight test maneuvers of a fighter aircraft. The second nonlinear system (Ref. 8) was an artificial neural network trained to reproduce the aerodynamic characteristics of a rapidly pitching wing undergoing dynamic stall. Reference 1 demonstrated the feasibility of the nonlinear indicial response approach. The method was shown to be considerably more accurate than aerodynamic stability derivatives-based approaches for unsteady flow. The method was also considerably faster than computational fluid dynamics (CFD) methods and became increasingly accurate as more indicial functions became available. Thus, an important conclusion of these earlier studies was that nonlinear indicial theory (Refs. 9,10) offers a viable solution which can fulfill the need for efficient and accurate modeling of nonlinear "plant" characteristics. The knowledge of these characteristics is a prerequisite for structural response feedback techniques and control system configuration design.

2. OBJECTIVE AND APPROACH

The goal of the present study (Ref. 11) was to provide an unsteady aerodynamic modeling capability based on nonlinear indicial theory. This goal was to be accomplished through two main tasks. The first task was to extend the nonlinear indicial prediction capability developed in Reference 1 by improving functional interpolation, extending the capability for multidimensional parameterization, and by adding the capability to handle multiple critical-state crossings. The second task was to produce a "companion code," which would be capable of extracting the indicial and critical-state responses from existing data. Together, these two codes would form the "Indicial Prediction System." The first component of the system constructs a nonlinear response based on prerecorded indicial and critical-state functions. The resulting nonlinear prediction can be generated inexpensively and for arbitrary inputs. The second component of the system extracts from experimental data the indicial and critical-state responses which must be fed into the prediction model.

To achieve the stated objectives, the following methods were used. The development of the extraction portion of the Indicial Prediction System was first tested against a variety of "synthetic data" (for which an exact answer is known), the complexity of which was increased in a systematic manner. The robustness and convergence properties of the extraction method (Ref. 12) were then evaluated through parametric changes in data content, noise characteristics, and the parameters of the extraction itself. The method was subsequently applied to real aerodynamic data (65-degree delta wing at 30 degrees angle of attack), where its robustness was once again verified by (a) filtering the data to various degrees and (b) perturbing the content of the training data subsets.

For the prediction portion of the Indicial Prediction System, comparisons were made, whenever possible, to exact, analytical answers. When analytical solutions were not available, the computed predictions were compared to numerically generated ones, using separate computational capabilities (for example, the calculations generated in Ref. 4). In particular, the nonlinear predictions of the Indicial Prediction System were validated against both the neural network and Goman-Khrabrov systems examined in Phase I (Refs. 3 and 2, respectively). Of particular relevance to the validation effort was the availability of Myatt's NIR model (Ref. 5) of the rolling moment for the 65-degree wing configuration, which was used extensively for this purpose (see Ref. 6).

The objective of this paper is to present the results of applying the complete system (consisting of both the extraction and prediction capabilities) to the rolling moment, pitching moment, and normal force coefficients of the 65-degree delta wing.

This application of the Indicial Prediction System is intended as a demonstration of the use of the system as a whole. Section 3 gives a brief theoretical introduction. This is followed by the Results section, which is organized as follows. First, the parameter space partitioning based on the quasi-static data is described. The various data processing steps are then given. Section 4.3 details the extraction procedure and the nonlinear indicial response model used. The results include extracted indicial and critical-state responses, the error metrics of the prediction, and predictions of novel maneuvers. The details of the extraction method can be found in a companion paper, Reference 12.

3. THEORY AND PREDICTION METHOD

Nonlinear indicial response (NIR) theory (Refs. 9,10) was developed to address the need for high-fidelity prediction of nonlinear unsteady aerodynamics. By representing the build-up of the aerodynamic loads using a generalized

superposition integral which accounts for the effects of flow bifurcations, nonlinear indicial theory provides a tool to understand and address nonlinear aspects of flight mechanics problems, particularly motion history effects. Nonlinear indical theory is a conceptually attractive tool because it has been shown (Ref. 13) that the nonlinear indicial response can, under certain conditions, be derived from the Navier-Stokes equations.

The theoretical derivations can be found in a number of references, for instance Refs. 3, 6, and 12. The present application of nonlinear indicial theory incorporates simplifications which have permitted its implementation in a versatile computer program, the Indicial Prediction System (IPS), Ref. 14. These simplifications assume that the indicial and critical-state responses can be parameterized based on the motion state at the time these responses are initiated, which is not to be confused with the relationship between the aerodynamic forces themselves and the prior motion history. Indeed, the present simplifications, which result in a parameterized, nodal representation of the indicial and critical-state responses, are entirely compatible with the notion that the nonlinear aerodynamic loads at moderate and high angles of attack are highly dependent on motion history.

The core mathematical function performed by IPS is that of calculating the build-up in a dependent variable DEP_i as

$$\Delta DEP_i(t) = \sum_{j=1}^{nDOF} \int_0^t IR_{ij}(t-\tau)\dot{DOF}_j(\tau)\,d\tau \qquad (1)$$

where the DOF_j are the participating degrees of freedom for DEP_i, and where each IR_{ij} is the so-called "indicial response" of DEP_i with respect to DOF_j. The slashed integral sign notation is intended to represent the fact that the integral must be split at critical-state encounters, and that at these points, a critical-state response (jump response) CSR_{ij} must be added. Each function IR_{ij} can be thought of as the time-dependent analog of the aerodynamic derivative of DEP_i with respect to DOF_j. Note that the indicial and critical-state responses in IPS are parameterized responses. The IPS methodology provides a great deal of flexibility in defining what these parameters are. In principle, the parameters can be independent variables, dependent variables, combination groups thereof, or alternate variables. They can be discrete or continuous, and can be defined in arbitrary numbers. Thus, true unsteady (motion history) effects are accounted for by the device of a generalized convolution integral (**Eq. (1)**); however, IR_{ij} and CSR_{ij} parameterizations are based on the parameter values calculated *at the time these responses are initiated* (in other words, parameters must be calculated at time τ, and not $(t-\tau)$ or t.

The Indicial Prediction System performs two main tasks, one of which is concerned with the direct problem and the other with the inverse problem. The direct problem is that of calculating the response of a nonlinear system, once its indicial and critical-state responses are known. The inverse problem consists of determining the system's kernel of nonlinear indicial and critical-state responses, based on observed data. In general, the indicial and critical-state responses of a nonlinear system can be determined by computational, experimental, or theoretical means, whichever are appropriate or available. Thus, the complete system addresses the following needs:

- High-fidelity prediction of nonlinear plant characteristics
- Ability to include empirical knowledge into the system
- Ability to be "trained" on known input-output transfer function characteristics

The latter capability (inverse problem) was implemented in IPS by means of a robust extraction technique based on the method of singular value decomposition. This extraction module was validated extensively against synthetic data, both with and without noise. The method was shown to behave robustly in synthetic data tests and in tests where various amounts of filtering were used on experimental data. Most importantly, the extracted indicial and critical-state responses were shown to converge with successive enrichments of the training data sets (Ref. 12).

4. APPLICATION TO THE 65-DEGREE DELTA WING

The 65-degree delta wing database provides an excellent test bed for the testing of nonlinear indicial response models. The database was collected as part of a joint program involving the U.S. Air Force Research Laboratory (formerly USAF/WL) and the Canadian Institute for Aerospace Research (IAR). As a result of this program, a wealth of unsteady aerodynamic responses are available for a variety of motions and flow conditions. Although the database includes other Mach numbers (M) and body axis angles (σ) with respect to the freestream, the results presented here are for the conditions M = 0.3 and $\sigma = 30^\circ$. The maneuvers under consideration are forced rolling motions $\phi(t)$. The available aerodynamic force and moment coefficient time histories include the rolling moment C_l, pitching moment C_m, normal force coefficient C_N, yawing moment C_n, and side force C_Y. The motions include both harmonic motions of various mean angle, amplitude and frequency, and ramp-and-hold motions of various rates and initial and final roll angles. A schematic of the wing model is shown in **Figure 1**.

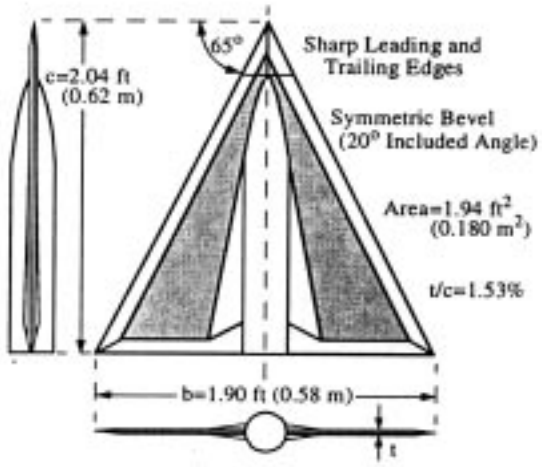

Fig. 1 Delta Wing Model Geometry (from Ref. 5).

Aside from the wealth of unsteady aerodynamic data available, the case of the rolling 65-degree wing at high angles of attack is interesting because it incorporates complex flow physics and flow state transitions (**Figure 2**) which are associated with considerable time lags with respect to the forcing motion. An additional benefit is that flow physics are reasonably well-understood and that the characteristics of the flow are well-documented (Refs. 15-18).

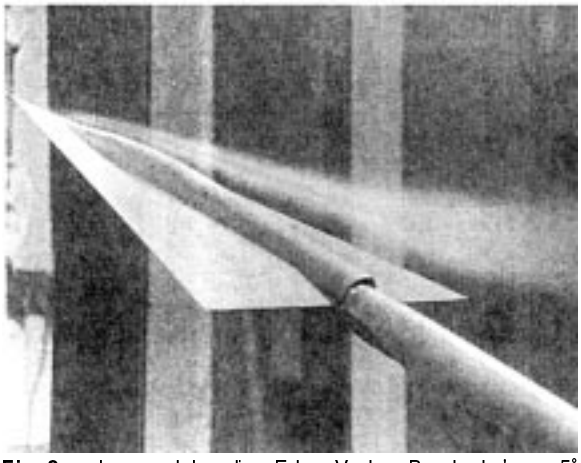

Fig. 2 Leeward Leading-Edge Vortex Burst at ϕ = -5° (from Ref. 16).

4.1 Static Data and Partitions

From previous analysis of flow visualization results and force and moment discontinuities, the roll angle range is split into seven regions:

$$
\begin{aligned}
&\textit{Region I} && : && -4.05^\circ \le \phi < 5^\circ \\
&\textit{Region II} && : && 5^\circ \le \phi < 8.5^\circ \\
&\textit{Region III} && : && 8.5^\circ \le \phi < 11.3^\circ \\
&\textit{Region IV} && : && 11.3^\circ \le \phi \\
&\textit{Region V} && : && -8.3^\circ \le \phi < -4.05^\circ \\
&\textit{Region VI} && : && -11.0^\circ \le \phi < -8.3^\circ \\
&\textit{Region VII} && : && \phi < -11.0^\circ
\end{aligned}
$$

The static (time-averaged) coefficient data are shown in **Figure 3** for C_l, C_m, and C_N. Within each region or partition, the data are fitted using low-order polynomials.

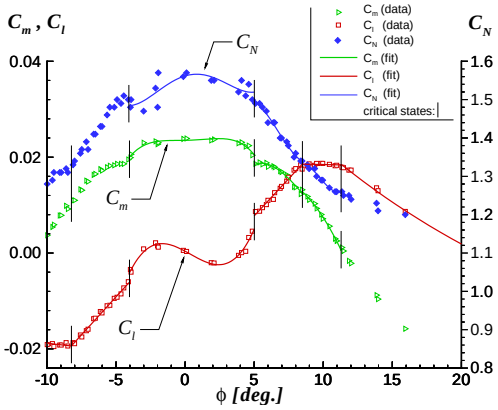

Fig. 3. Polynomial Fits to Static Force and Moment Coefficient Data.

4.2 Data Processing

As previously mentioned, the available unsteady data include both harmonic excitation and ramp-and-hold types of rolling motions. The data processing steps differ, depending on motion type. Each is described in the following subsections, which discuss the successive steps of data preparation for the purpose of extraction: *(i)* "raw" data, *(ii)* low-pass filtering, and *(iii)* dynamic data component.

4.2.1 Preparation of "Raw" Data

The harmonic data consisted of phase-averaged data. The number of realizations used for phase-averaging was on the order of 20, consistent with previous studies (Refs. 15,18). The resulting data are assumed to be phase-locked to the excitation and are referred to here as the "raw" or "unfiltered" data.

The ramp-and-hold data were processed in accordance with the methodology previously developed by Grismer and Jenkins (Ref. 16). This multistep process can be summarized as follows. The force balance is first calibrated. Tare and wind-on data are then calibrated and low-pass filtered. The cut-off frequency of the low-pass filtering was determined based on comparisons of the wind-

on and wind-off data for a number of maneuvers. The frequency cut-off was 145 Hz for the normal force and pitching moment coefficients, and 100 Hz for the rolling moment and the roll angle. The inertial effects for the rolling moment coefficient were determined based on the tare runs by exploiting the expected correlation between the twice-differentiated roll angle and the rolling moment (Ref. 17). This required specialized processing to infer the roll angle at the balance center, which is where the rolling moment was measured. Once the inertial effects were determined, they were subtracted from the wind-on measurements in order to obtain the aerodynamic loads. The resulting force and moment coefficient data are what are referred to here as the "raw" data (also referred to as "unfiltered" data, for reasons of consistency with the harmonic data and further processing steps, see below).

4.2.2 Low-Pass Filtering

In order to investigate the sensitivity-to-noise of the extraction method (Ref. 12), it has been necessary to experiment with various levels of smoothing of the data. This further data processing step was carried out as follows. For harmonic motions, the data were Fourier analyzed and a fixed number of harmonics of the fundamental excitation frequency were retained. For ramp-and-hold motions, the employed methodology was the same as that previously used by Myatt (Ref. 19). First, the data were reflected to define artificially a fundamental period. Then, the data were Fourier decomposed, and a specific number of harmonics of the fundamental were retained.

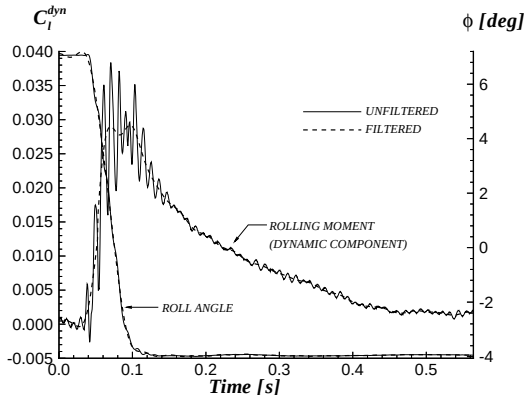

Fig. 4. Filtered and Unfiltered Dynamic Rolling Moment Response for +7° to +4° Ramp-and-Hold Motion (Maximum Roll Rate: 4 rad/s).

It was found in the present study that the low-pass filtering on the harmonic data had a more consistent effect if, instead of maintaining the number of harmonics constant for a given set of data, the upper frequency were kept constant. This was done in each case by automatically adjusting the number of retained harmonics so as to achieve the desired bandwidth. For extraction purposes, the training data consist of a mixture of harmonic and ramp-and-hold data. Note: the terminology used here is that a "64-harmonic" case actually refers to: *(i)* 64 retained harmonics for the ramp-and-hold data and *(ii)* a bandwidth of 64 Hz for the harmonic data. Unless otherwise specified, the data used for training is 32-harmonic. An example of "raw" and low-pass filtered data is given in **Figure 4** for the case of a ramp motion from $\phi = 7^\circ$ to $\phi = 4^\circ$.

4.2.3 Dynamic Data Component

The extraction method described in Ref. 12 identifies deficiency responses, rather than indicial responses. (The deficiency response is the indicial response, minus its time-asymptotic value). Likewise, the results of the critical-state response extraction are really the dynamic component of the critical-state responses (loosely referred to as critical-state deficiency response, CSDR). For this reason, it is the *dynamic* component of the data which must be supplied for purposes of extraction. This dynamic component is obtained by subtracting the quasi-static or time-averaged component from the data. To avoid noisy estimates of the dynamic component the quasi-static component at a given roll angle is taken to be the value of the fit to the static data (**Figure 3**). Note: it is important that the subtraction of the static load curves be carried out last, in order to retain sharp jumps at the critical states.

4.3 Extraction Procedure

The present section is used to describe the steps taken to extract the indicial and critical-state responses for the 65-degree delta wing.

4.3.1 NIR Model

The indicial model that was constructed is designed to be valid in Regions I through VII ($-30^\circ < \phi < 30^\circ$) for the rolling moment C_l, and Regions I, II, and III ($-4.05^\circ < \phi < 11.3^\circ$) for the pitching moment C_m and normal force C_N. All IR/CSR extractions carried out (i.e., of C_l with respect to ϕ, of C_m with respect to ϕ, and of C_N with respect to ϕ) are generically denoted $\delta C_x/\delta\phi$. A common parameterization of the $\delta C_x/\delta\phi$ IR/CSR space was used, where each indicial or critical-state response is parameterized by the instantaneous roll angle, ϕ, and the sign of the instantaneous roll rate, $sgn(d\phi/dt)$. Thus, there are two critical-state responses per partition transition (one for positive roll rate and one for negative roll rate), for a total of 12 critical-state responses. Within each partition, the indicial response nodes were laid out at regular intervals, as shown in **Figure 5**. Because of the dual parameterization, there are actually two indicial response nodes per roll angle, for a total of 38 indicial responses (for C_l).

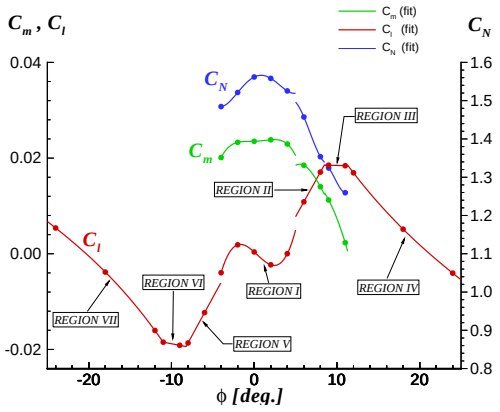

Fig. 5 Overlay of *(i)* Analytical Fits to the Static Data and *(ii)* Nodal Indicial Response Locations.

4.3.2 Basis Functions

The extraction of deficiency responses requires their expansion on some basis function set, $f_j(t)$. All IR/CSR extractions used a common set of exponential basis functions, defined as

$$f_j(t) = \exp(-8jt),\ j = 1,\ldots,8 \qquad (2)$$

This choice of basis functions was designed to bracket time constants ranging between 1/8 = 0.125 seconds (for j = 1) and 1/64 = 15.6 milliseconds (for j = 8).

4.3.3 Training Data

The extraction results were obtained in stages, using only small amplitude maneuvers. The latter are defined as rolling motions for which the roll angle time history spans at most two partitions.

The staged extraction methodology was carried out as follows. The indicial responses of Region I were extracted first, using maneuvers confined to Region I. The critical-state responses between Regions I and II as well as the indicial responses in Region II were then extracted using motions confined only to Region I and Region II. The motions whose trajectories visit Regions II and III were then used to extract the Region III IR nodes, as well as the CSR nodes between Regions II and III, and so on.

In this manner, 28 IR nodes and 8 CSR nodes, corresponding to Regions I through V, were extracted for C_l (similarly: 18 IR nodes and 4 CSR nodes, corresponding to Regions I through III, for C_m and C_N). Since the static rolling moment response is, nominally, an antisymmetric function of the roll angle, the $\delta C_l/\delta\phi$ nodes involving Regions VI and VII were obtained by mirroring. This procedure was necessary because of the lack of small amplitude data in these regions. The mirroring operation involved a symmetric reflection about zero for the dynamic portion of the indicial responses and an antisymmetric reflection about zero for the critical-state response deficiency responses (CSDR):

$$CSDR_{VI\to VII}(t) = -CSDR_{III\to IV}(t)$$
$$CSDR_{VII\to VI}(t) = -CSDR_{IV\to III}(t) \qquad (3)$$

No special treatment was required for the static components of these responses, since the time-asymptotic value of the indicial response is the value of the static slope $dC_x/d\phi$, as determined from the analytical fit to the static data. Similarly, the time-asymptotic value of critical-state responses is determined on the basis of the static discontinuities, if any, of the analytical fits across partitions.

A summary of the number of training maneuvers used at each stage of the extraction, along with their breakdown according to whether the motions are periodic or ramps, is given in **Table 1**.

Region	#IRs	#CSRs	Basis Coeff.	Training Data Sets		
				Total	Harm.	Ramp
I	10	0	80	**18**	15	3
II	4	2	48	**39**	20	19
III	4	2	48	**25**	4	21
IV	6	2	64	**48**	32	16
V	4	2	48	**23**	0	23
VI	4	2				
VII	6	2				

Table 1. Number of Training Maneuvers Per Stage of the Extraction.

A total of 153 maneuvers (for C_l) was used for training out of a total of 650 available maneuvers.

Table 1 also gives the number of basis function coefficients which each stage of the extraction yielded (that number is the number of nodal (IR and CSR) responses to be extracted, times the number of basis functions). As a general rule, the number of available maneuvers dictates the amount of information (i.e., the number of basis coefficients) that can be extracted. If N maneuvers yield γN pieces of information on average (for an individual data set, the yield γ is the number of significant eigenvalues of the motion matrix, see Ref. 12), the NIR model design and extraction must take this constraint into account, such that

$$number\_of\_nodes \times number\_of\_basis\_functions \le \gamma N$$

If the motions are pure harmonic, it can be shown that γ = 2. In the case of the 65-degree delta wing, the motions are a mixture of harmonic and ramp-and-hold motions, and

the yield factor γ was empirically estimated at approximately 4 for this particular data base.

4.4 Results

This section documents the results of the extraction procedure. The raw results, namely, the extracted indicial and critical-state responses are shown first. This is followed by an error metrics analysis, which involves the prediction of the training data from the extracted responses. Finally, the extracted IR and CSR are used for the prediction of novel data. Unless otherwise specified, the results correspond to the 32-harmonic rolling moment coefficient.

4.4.1 Extracted Responses

Indicial Responses. A sample of the extracted deficiency responses is given in **Figures 6** through **9**. **Figures 6**, **7**, and **8** correspond, respectively, to the nodal locations ϕ = 0˚, ϕ = 4˚, and ϕ = 8˚. Each figure depicts three responses: the extracted response for positive roll rate, the extracted response for negative roll rate, and the deficiency response corresponding to Myatt's NIR model (Refs. 5,19), which is included for reference.

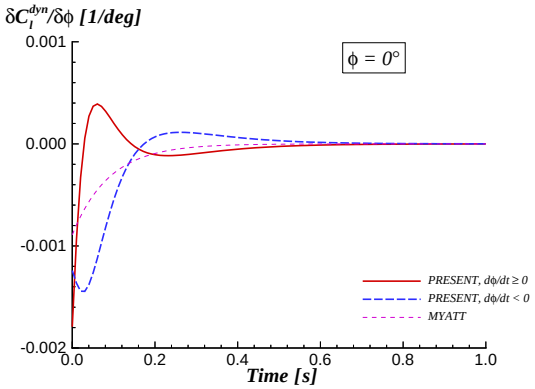

Fig. 6 Extracted Rolling Moment Deficiency Responses at ϕ = 0˚.

Significant differences can be observed at ϕ = 0˚ and ϕ = 8˚ between the time constants for positive roll rate and negative roll rate. It is also interesting to notice, for these cases, that the deficiency response corresponding to Myatt's model appears to lie somewhere in between the positive and negative roll rate responses. This is, perhaps, not surprising, since, in Myatt's model, the indicial responses are parameterized by roll angle only, irrespective of roll rate. At ϕ = 4˚ the differences between positive and negative roll rates are reduced and, correspondingly, good agreement is found with Myatt's response.

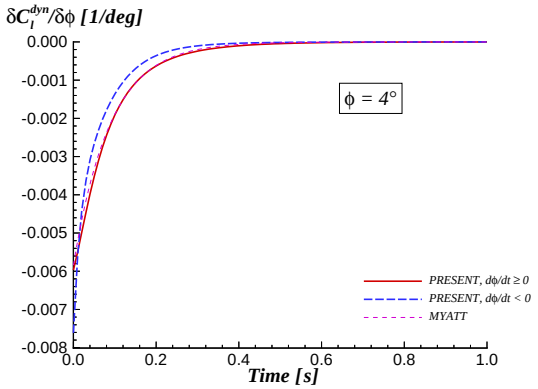

Fig. 7 Extracted Rolling Moment Deficiency Responses at ϕ = 4˚.

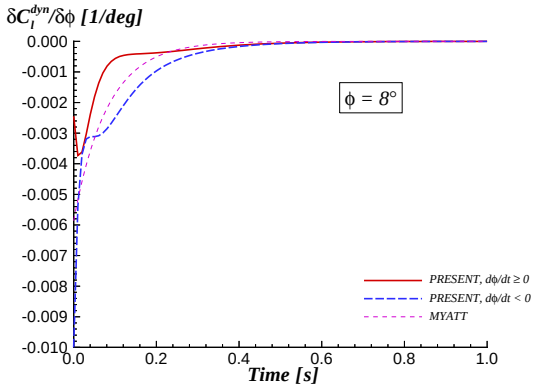

Fig. 8 Extracted Rolling Moment Deficiency Responses at ϕ = 8˚.

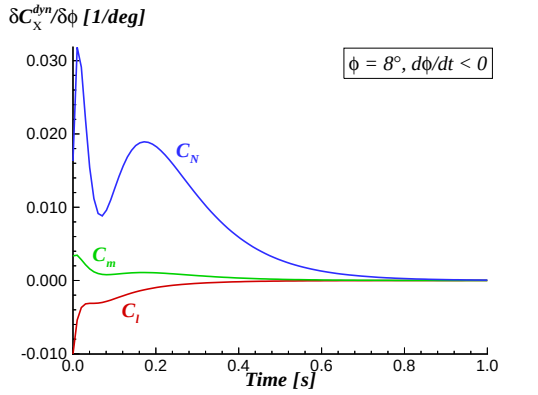

Fig. 9 Comparison of Extracted Deficiency Responses for C_l, C_m, and C_N at ϕ = 8˚, dϕ/dt < 0.

Similar results have been obtained for the pitching moment and normal force coefficients, although these cannot be compared against Myatt's model (which is for C_l only). For

reference, **Figure 9** shows the extracted deficiency responses for C_l, C_m, and C_N for ϕ = 8˚ and negative roll rate. Note that the variety of shapes and apparent time constants is obtained with the same set of basis functions.

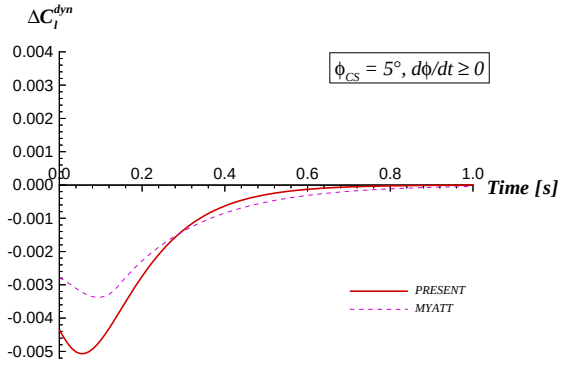

Fig. 10 Extracted Critical-state Response at ϕ_{CS} = 5˚, Positive Roll Rate.

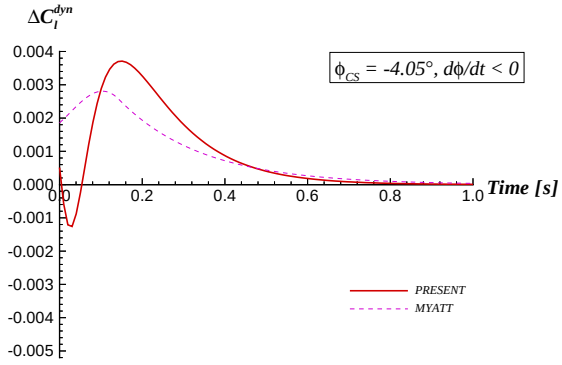

Fig. 11 Extracted Critical-state Response at ϕ_{CS} = -4.05˚, Negative Roll Rate.

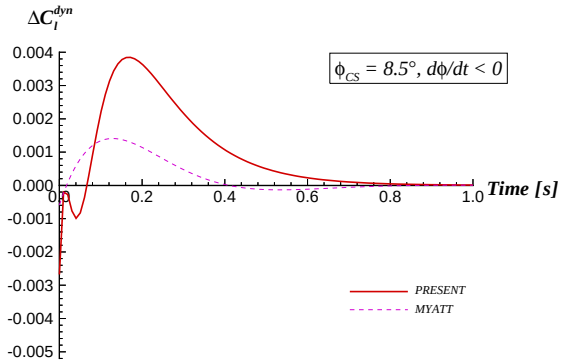

Fig. 12 Extracted Critical-state Response at ϕ_{CS} = 8.5˚, Negative Roll Rate.

Critical-state Responses. A sample of the extracted dynamic component of the critical-state responses is shown in **Figures 10** through **13**. The first three figures correspond to the rolling moment critical-state response. **Figures 10** and **11** depict the dynamic jump response incurred when the wing rolls from Region I to Region II, and from Region I to Region V, respectively. **Figure 12** corresponds to the critical-state encounter from Region III to Region II. (For a discussion of the physical meaning of these critical-state transitions, see Reference 16).

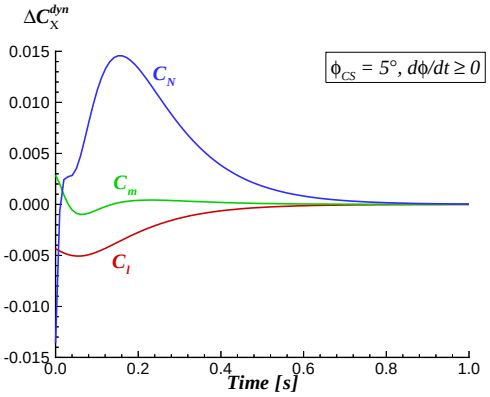

Fig. 13 Extracted Critical-states Response for C_l, C_m and C_N at ϕ_{CS} = 5˚ and Positive Roll Rate.

A rough estimate of time constants associated with the various critical-state responses is given in **Table 2**. Since the responses are not of exponential type, the so-called "time constants" were determined as the time it takes for the dynamic CSR component to decay 63% from its peak value. This time was measured from the peak time and, in the event of multiple extrema, the peak corresponded to the last local extremum (i.e., the measure characterizes the final period of decay). While somewhat subjective, this measure was applied consistently across the range of extracted responses and is compared in **Table 2** to Myatt's results.

Critical State	Time Constant	
	present	Myatt
I → II	0.3	0.32
II → I	0.38	0.51
II → III	0.59	0.3
III → II	0.51	0.29
III → IV	0.22	--
IV → III	0.27	--
V → I	0.31	0.54
I → V	0.37	0.33

Table 2. Estimate of Time Constants for Various Critical-state Responses.

All numerical values in **Table 2** are in seconds. The time constants between Region I and its neighbors (Region II for positive roll rate and Region V for negative roll rate) are similar to those in Myatt's model. However, the reverse transitions *into* Region I do not appear to exhibit the longer time constants found by Myatt. The extracted time constants associated with the extracted CSRs between Regions II and III are almost double those of Myatt's model, while the extracted CSRs between Regions III and IV have a smaller but nonnegligible response time.

A comparison of the simultaneous critical-state responses for the different force and moment coefficients is shown in **Figure 13** for ϕ_{CS} = 5°, positive roll rate.

4.4.2 Error Metrics

In order to determine how good a fit the extracted NIR model is with respect to the data, the extracted indicial and critical-state responses can be used to predict the maneuvers that were used for the extraction. An example of this prediction is shown in **Figure 14**. In this figure, the prediction based on the extracted indicial and critical-state responses (labeled *PRESENT*) is compared to the data (symbols). Myatt's prediction is also indicated for reference.

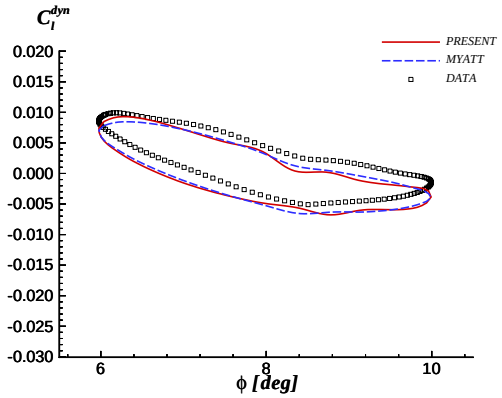

Fig. 14 Prediction of Dynamic Rolling Moment, Harmonic Motion, $\Phi = 8^\circ \pm 2^\circ$, f = 2.2 Hz.

The error metrics are calculated either as the norm-1 ($\lhd$ predicted − data | >) or norm-2 (<(predicted − data)^2>$^{1/2}$) error between the model prediction and the data, computed over all training maneuvers used within a given stage of the extraction. The error was computed using 32 points per maneuver, equally spaced in time. A summary of the error metrics results is given in **Table 3**.

Extraction Stages	Number of Maneuvers	NIR model	Error Metrics	
			L1-norm	L2-norm
Region I	18	present	0.00051	0.00063
		Myatt	0.00107	0.00124
Region I-II	39	present	0.00163	0.00227
		Myatt	0.00293	0.00419
Region II-III	25	present	0.00124	0.00147
		Myatt	0.00148	0.00161
Region III-IV	48	present	0.00129	0.00167
		Myatt	0.00128	0.00168
Region I-V	23	present	0.00097	0.00127
		Myatt	0.00142	0.00170

Table 3. Summary of Error Metrics for the Rolling Moment Coefficient.

A comparison of the error metrics between the different force and moment coefficients is provided in **Table 4**. This time the error is computed over all 82 maneuvers used in the extraction of Regions I, II, and III.

Force Coefficient	**Error Metrics**	
	L1-norm	**L2-norm**
Rolling Moment	0.00090	0.00128
Pitching Moment	0.00129	0.00186
Normal Force	0.01555	0.01678

Table 4. Summary of Error Metrics in Regions I, II, and III.

The error was observed to be consistently larger on the pitching moment, as compared to the rolling moment. It is conjectured this may be caused by a smaller deterministic (phase-locked) signal component for C_m. The absolute error is largest for C_N; however, the values of C_N variations are also an order of magnitude larger, so that the extraction performance, in terms of fitting the training data, is approximately similar to the rolling moment.

4.4.3 Novel Maneuvers

The error metrics results described in the previous section imply that the extracted NIR model is a valid fit to the training data, which is a necessary condition. However, the true test of the usefulness of the method is its ability to predict novel maneuvers, i.e., maneuvers that were not included in the extraction. **Figures 15** through **20** provide a representative sample of the predicted dynamic rolling moment for novel maneuvers.

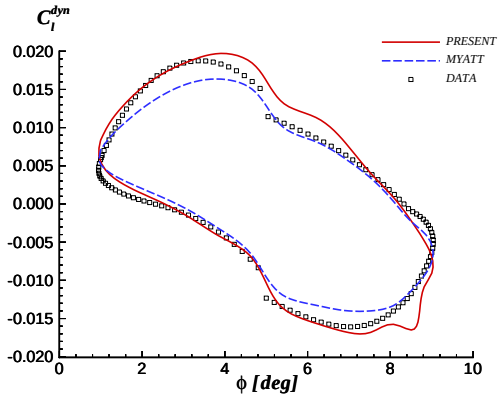

Fig. 15 Prediction of Dynamic Rolling Moment, Harmonic Motion, Φ = 5°±4°, f = 1.1 Hz.

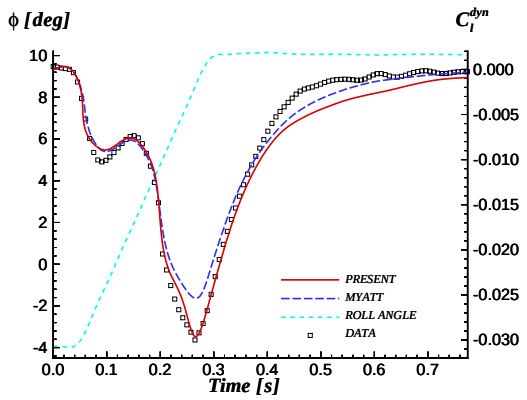

Fig. 18 Prediction of Dynamic Rolling Moment, Ramp-and-Hold Motion, Φ = -4°→10°, 1 rad/s.

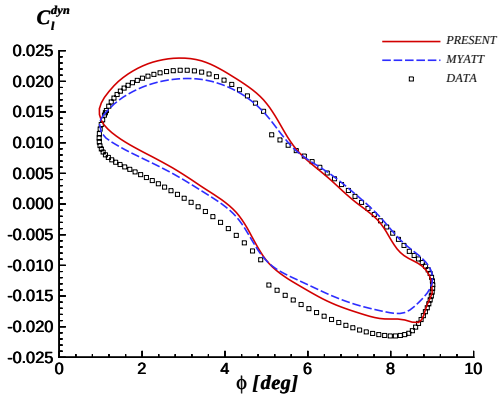

Fig. 16 Prediction of Dynamic Rolling Moment, Harmonic Motion, Φ = 5°±4°, f = 2.2 Hz.

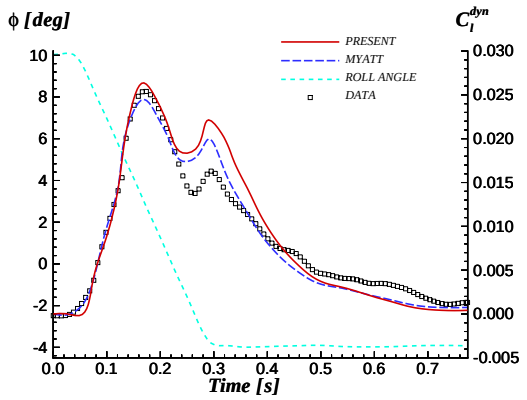

Fig. 19 Prediction of Dynamic Rolling Moment, Ramp-and-Hold Motion, Φ = 10°→-4°, −1 rad/s.

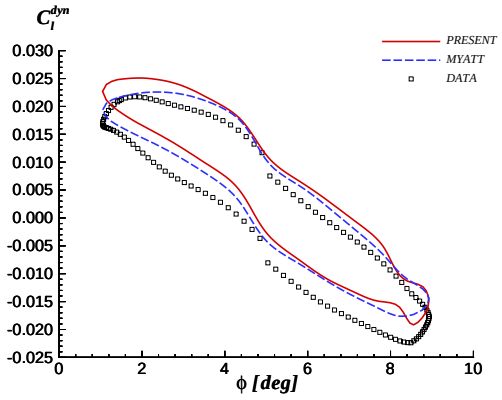

Fig. 17 Prediction of Dynamic Rolling Moment, Harmonic Motion, Φ = 5°±4°, f = 4.4 Hz.

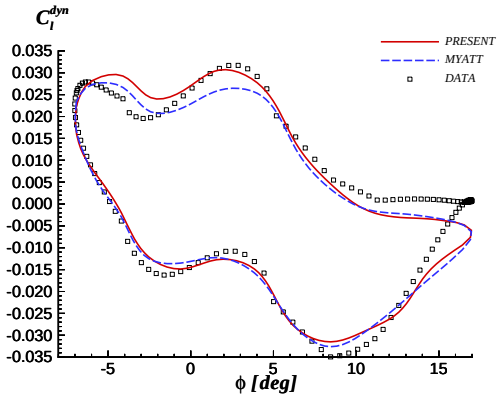

Fig. 20 Prediction of Dynamic Rolling Moment, Harmonic Motion, Φ = 5°±12°, f = 1.1 Hz.

Figures 15 through **17** correspond to harmonic motions of eight degrees peak-to-peak amplitude, centered at five degrees roll angle. The difference between these motions is the frequency of excitation. In each case, the motion trajectory crosses two critical states, so that the calculation involves four critical-state responses (two for positive roll rate, and two for negative roll rate) and, naturally, their various echoes depending on the excitation frequency. Thus, the calculation of **Figure 15** involves contributions from four critical-state encounters. The calculation of **Figure 16** requires keeping track of as many as nine critical-state encounters. That number is increased to 18 critical-state encounters in the case of **Figure 17**.

Figures 18 and **19** similarly involve the crossing of two critical states (one at ϕ_{CS} = 5˚ and one at ϕ_{CS} = 8.5˚), except that these are only crossed once in the case of ramp maneuvers.

Figure 20 corresponds to a large-amplitude harmonic motion (24 degrees peak-to-peak) centered at five degrees roll angle. Consequently, the motion trajectory visits five partitions and crosses four critical states. At the low frequency of the excitation, the calculation requires keeping track of eight critical-state encounters.

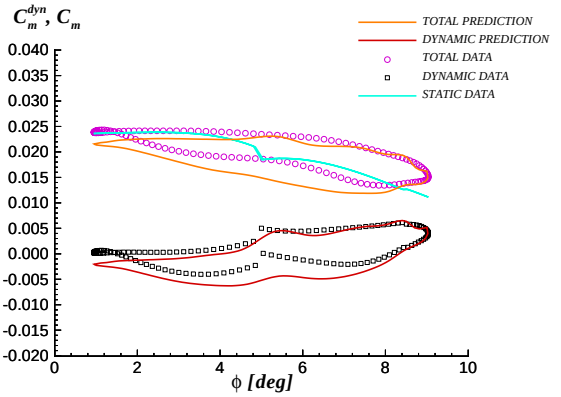

Fig. 21 Prediction of Dynamic and Total Pitching Moment, Harmonic Motion, Φ = 5°±4°, f = 1.1 Hz.

For completeness, novel prediction results for different force and moment coefficients are shown in **Figures 21**, **22**, and **23**. The lower curves and symbols in these figures correspond to the dynamic component. The upper curves and symbols correspond to the total response (i.e., dynamic plus quasi-static).

The results of **Figures 15** through **23** illustrate the method's ability to predict the loads associated with novel maneuvers, suggesting that the extraction method does indeed identify the response kernel of the system.

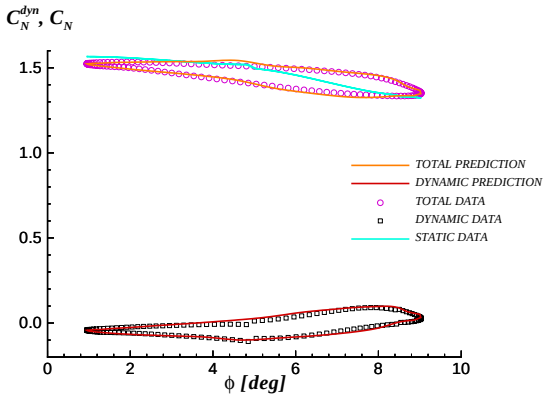

Fig. 22 Prediction of Dynamic and Total Normal Force, Harmonic Motion, Φ = 5°±4°, f = 1.1 Hz.

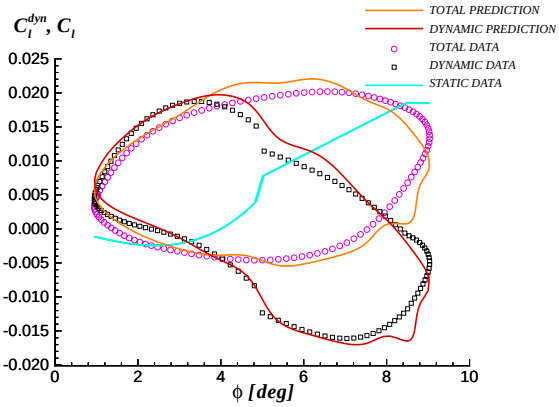

Fig. 23 Prediction of Dynamic and Total Rolling Moment, Harmonic Motion, Φ = 5°±4°, f = 1.1 Hz.

5. SUMMARY

The necessity to reduce cost of ownership of aircraft has led, in the past several years, to considerable efforts aimed at accelerating the design cycle, and the ability to understand, model, and incorporate early the knowledge of aerodynamic nonlinearities is considered critical to this effort. Nonlinear indicial response technology has the potential to provide fast, yet high-fidelity aerodynamics, which is needed for use in preliminary design and flight simulation applications.

The present implementation of nonlinear indicial theory makes certain simplifications which allow the representation of the system's kernel of indicial and critical-state responses in a parameterized nodal form. A benefit of such a representation is that it is possible to carry out the inverse problem of identifying the kernel (i.e., the *internal structure*) of the physical (aerodynamic) system, based on the system's measured behavior. The extraction method is described in the companion to this paper, Reference 12.

The prediction component of the Indicial Prediction System was previously validated (Refs. 2-6) against prior implementations of nonlinear indicial theory, which included the following: **(1)** simulated roll response of a delta wing at high angle of attack, **(2)** "cobra" maneuver of a fighter aircraft, **(3)** neural network system for dynamic stall, and **(4)** Myatt's NIR model of the rolling moment of the 65-degree delta wing. The present paper describes the application of the complete system (extraction and prediction) to the aerodynamic loads of a 65-degree delta wing undergoing forced rolling motions at a body axis angle of 30 degrees to the freestream and a Mach number of three-tenths. Specifically, nonlinear indicial and critical-state responses are extracted for the rolling moment C_l, pitching moment C_m, and normal force coefficient C_N. It is shown that these, in turn, can be used to accurately predict the time-dependent aerodynamic loads associated with novel maneuvers.

ACKNOWLEDGMENT

The authors gratefully acknowledge the support of this work by the Air Force Research Laboratory Aeronautical Sciences Division under Phase II SBIR Contract F33615-96-C-3613.

REFERENCES

1 Reisenthel, P. H.: Novel Application of Nonlinear Indicial Theory For Simulation and Design of Maneuvering Fighter Aircraft, WL-TR-95-3094, Dec. 1995.

2 Reisenthel, P. H.: Development of a Nonlinear Indicial Model For Maneuvering Fighter Aircraft, AIAA Paper 96-0896, Jan. 1996.

3 Reisenthel, P. H.: Application of Nonlinear Indicial Modeling to the Prediction of a Dynamically Stalling Wing, AIAA Paper 96-2493, Jun. 1996.

4 Reisenthel, P. H.: Development of a Nonlinear Indicial Model Using Response Functions Generated by a Neural Network, AIAA Paper 97-0337, Jan. 1997.

5 Myatt, J. H.: Modeling the Rolling 65-Degree Delta Wing with Critical State Encounters, AIAA Paper 97-3646, Aug. 1997.

6 Reisenthel, P. H., Bettencourt, M. T., Myatt, J. H., and Grismer, D. S.: A Nonlinear Indicial Prediction Tool for Unsteady Aerodynamic Modeling, AIAA Paper 98-4350, Aug. 1998.

7 Goman, M. and Khrabrov, A.: "State-Space Representation of Aerodynamic Characteristics of an Aircraft at High Angles of Attack," *J. Aircraft*, Vol. 31, No. 5, 1994, pp. 1109-1115.

8 Faller, W. E., Schreck, S. J., and Luttges, M. W.: Real-Time Prediction and Control of Three-Dimensional Unsteady Separated Flow Fields Using Neural Networks, AIAA Paper 94-0532, Jan. 1994.

9 Tobak, M., Chapman, G. T., and Schiff, L. B.: Mathematical Modeling of the Aerodynamic Characteristics in Flight Dynamics, NASA TM 85880, 1984.

10 Tobak, M. and Chapman, G. T.: Nonlinear Problems in Flight Dynamics Involving Aerodynamic Bifurcations, NASA TM 86706, 1985.

11 Reisenthel, P. H. and Bettencourt, M. T.: Development of a Nonlinear Indicial Prediction System for Unsteady Aerodynamic Modeling, AFRL-VA-WP-TR-1998-3036, Jan. 1999.

12 Reisenthel, P. H. and Bettencourt, M. T.: Extraction of Nonlinear Indicial and Critical State Responses from Experimental Data, AIAA Paper 99-0764, Jan. 1999.

13 Truong, K. V. and Tobak, M.: Indicial Response Approach Derived from the Navier-Stokes Equations Part 1 - Time-Invariant Equilibrium State, NASA TM-102856, Oct. 1990.

14 Bettencourt, M. T. and Reisenthel, P. H.: Indicial Prediction System Version 1.0 - User's Manual, AFRL-VA-WP-TR-1998-3087, Jan. 1999.

15 Jenkins, J. E., Myatt, J. H., and Hanff, E. S.: "Body-Axis Rolling Motion Critical States of a 65-Degree Delta Wing," *J. Aircraft*, Vol. 33, No. 2, 1996, pp. 268-278.

16 Jobe, C. E., Hsia, A. H., Jenkins, J. E., and Addington, G. A.: "Critical States and Flow Structure on a 65-Deg Delta Wing," *J. Aircraft*, Vol. 33, No. 2, 1996, pp. 347-352.

17 Grismer, D. S. and Jenkins, J. E.: "Critical-State Transients for a Rolling 65° Delta Wing," *J. Aircraft*, Vol. 34, No. 3, May-Jun. 1997, pp. 380-386.

18 Jenkins, J. E.: Nonlinear Aerodynamic Characteristics of a 65° Delta Wing in Rolling Motion: Implications for Testing and Flight Mechanics Analysis, AIAA Paper 97-0742, Jan. 1997.

19 Myatt, J. H.: Modeling the Rolling Moment on the 65-Degree Delta Wing for Rolling Motions at High Angle of Attack, Ph.D. Dissertation, Department of Aeronautics and Astronautics, Stanford University, Apr. 1997.